JOURNAL OF GUIDANCE, CONTROL, AND DYNAMICS
Vol. 17, No. 6, November–December 1994

Optimal Lateral-Escape Maneuvers for Microburst Encounters During Final Approach

H. G. Visser*
Delft University of Technology, Delft, The Netherlands

This paper is concerned with the optimization of lateral-escape trajectories in a microburst wind field for an aircraft on final approach. The objective is to minimize the peak value of altitude drop. An extensive numerical effort has been undertaken to investigate the characteristics of open-loop extremal solutions for various locations of the microburst. When a sufficiently large aerodynamic roll-angle limit is specified and the center of the microburst is not too far offset from the centerline extension of the approach runway, typically three trajectories can be found that satisfy the first-order necessary conditions of optimality for a given set of boundary conditions, namely, a trajectory that passes the microburst center to the left, a trajectory passing the center to the right, and a trajectory passing right through the center. The results bear out that a lateral-escape maneuver, in which an aircraft is turned away from the microburst center, may significantly improve an aircraft's survivability, in comparison to an escape maneuver that is restricted to a vertical plane. One of the most striking observations in this study is that, in contrast to nonturning escape maneuvers, lateral-escape maneuvers often exhibit a climb, rather than a descent, in the initial phase. The insight obtained from the present study may help the development of near-optimal lateral-escape guidance strategies for onboard application.

I. Introduction

WEATHER phenomena that cause windshear, in particular the so-called microburst, present a significant safety hazard during the take-off and landing of an aircraft. Such a microburst is a strong downdraft that results in radially diverging winds near the ground (see Fig. 1). An airplane that penetrates the center of a microburst will initially experience an increasing headwind and consequent upward force. As the aircraft proceeds along the glide slope, the downdraft increases and the headwind shifts into a tailwind causing the aircraft to loose speed and altitude.

Reactive windshear-warning systems, which are gradually becoming standard fit aboard modern jet airliners, are capable of detecting such hazardous situations. When during final approach an aircraft is flying along the glide slope and such a potentially dangerous windshear situation is detected at a sufficiently early stage, the pilot may abort the landing and initiate an escape maneuver.

Research efforts that aim at establishing the optimal control strategy for such escape procedures have been conducted for some time now. However, most of these studies have focused on controlling and optimizing flight trajectories in a vertical plane. Of particular interest in this context is the work of Miele et al. In addition to considering control strategies to improve the take-off and penetration landing performance during microburst encounter,[1,2] Miele et al. also deal with the abort landing.[3] More specifically, Miele et al. consider optimal (open-loop) trajectories through windshears and downdraft that minimize the peak value of the altitude drop, as well as closed-loop guidance strategies that closely approximate these open-loop optimal trajectories.

Zhao and Bryson[4,5] propose an alternative formulation for the optimization of flight paths through microbursts. More specifically, paths are determined through windshears and downdrafts that maximize the final value of specific energy while taking into account a minimum-altitude constraint. It turns out that for strong to severe microbursts, the computed optimal paths are not essentially different from those found by Miele et al.

Hinton[6] has examined a set of candidate strategies for recovery from microburst encounter using both batch and piloted simulation. His findings indicate that improving the alert time by just a few seconds can already significantly improve the survivability during final approach.

Currently, substantial research efforts are being undertaken to develop so-called forward-looking windshear detection systems that allow to look ahead of the aircraft.[6,7] In addition to improving the alert time, the availability of the information on the location of a microburst also offers the possibility of applying escape procedures involving lateral maneuvering. By turning the aircraft away from the microburst center, rather than flying straight through, the hazards caused by the penetration of a microburst can be reduced. These potential improvements were recently confirmed by a simulation study[8] in which flights with and without lateral maneuvering were compared. In this simulation study, the longitudinal strategy as rec-

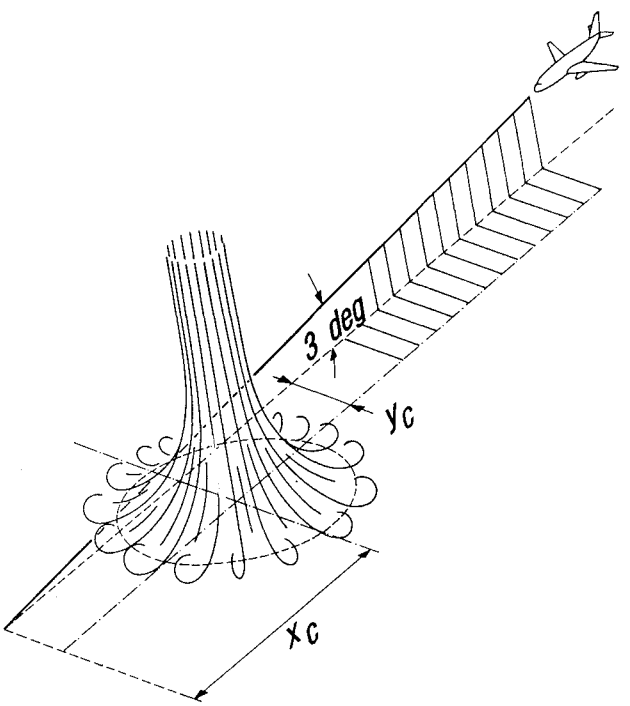

Fig. 1 Microburst encounter during final approach.

Received June 17, 1993; accepted for publication April 4, 1994.

*Lecturer, Faculty of Aerospace Engineering. Member AIAA.

ommended by the FAA windshear training aid[9] was used, whereas lateral maneuvering was performed by commanding a constant roll angle of specified magnitude.

Encouraged by these findings, the aim of the present study is to extend the work of Miele et al. by computing optimal abort landing trajectories that feature lateral maneuvering.

II. Microburst Encounter Modeling

Equations of Motion

Using a relative wind-axes reference frame, the equations of motion describing the aircraft dynamics (represented by a point-mass model) in the three-dimensional space can be written as

$$\dot{x} = V\cos\gamma\cos\psi + W_x \tag{1}$$

$$\dot{y} = V\cos\gamma\sin\psi + W_y \tag{2}$$

$$\dot{h} = V\sin\gamma + W_h \tag{3}$$

$$\dot{E} = \frac{\left\{T\left[1 - \frac{1}{2}(\alpha+\delta)^2\right] - D\right\}V}{W} + \dot{W}_h - \frac{V}{g}[\dot{W}_x\cos\gamma\cos\psi + \dot{W}_y\cos\gamma\sin\psi + \dot{W}_h\sin\gamma] \tag{4}$$

$$\dot{\gamma} = \frac{g}{V}\left[\frac{L + T(\alpha+\delta)}{W}\cos\mu - \cos\gamma\right] + \frac{1}{V}[\dot{W}_x\sin\gamma\cos\psi + \dot{W}_y\sin\gamma\sin\psi - \dot{W}_h\cos\gamma] \tag{5}$$

$$\dot{\psi} = \frac{g}{V\cos\gamma}\frac{L + T(\alpha+\delta)}{W}\sin\mu + \frac{1}{V\cos\gamma}[\dot{W}_x\sin\psi - \dot{W}_y\cos\psi] \tag{6}$$

$$\dot{\beta} = \frac{1}{\tau}[\beta_t - \beta] \tag{7}$$

where x, y, and h are the position coordinates; E is the specific energy; γ is the flight path angle; ψ is the heading angle; and β is the throttle response. The wind velocity vector has three components, viz., W_x, W_y, and W_h. The above equations embody the following assumptions: (1) a steady wind flow field and (2) a zero angle of sideslip. The thrust T is assumed to have a fixed inclination δ relative to the zero-lift axis. To simplify the optimal control analysis, a small-angle approximation has been employed in the equations of motion for the thrust components along and perpendicular to the airspeed vector respectively, i.e., $\cos(\alpha+\delta) \approx 1 - \frac{1}{2}(\alpha+\delta)^2$ and $\sin(\alpha+\delta) \approx \alpha + \delta$. The throttle response is modeled as a first-order lag with a time constant τ. Note that since specific energy E is used here as a state variable, the airspeed V should be merely regarded as a function of energy E and altitude h, to be obtained from the relation

$$E = h + \frac{V^2}{2g} \tag{8}$$

In the mathematical model the controls are (1) the throttle setting β_t constrained by

$$0 \le \beta_t \le 1 \tag{9}$$

(2) the aerodynamic roll angle μ, which is limited by

$$|\mu| \le \mu_{\max} \tag{10}$$

and (3) the angle of attack α, which is forced to remain within the range

$$0 \le \alpha \le \alpha_{\max} \tag{11}$$

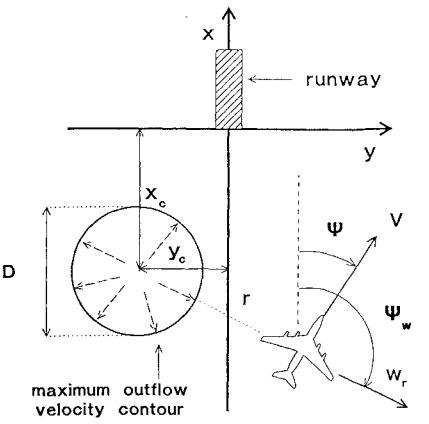

Fig. 2 Geometry of microburst encounter.

The aerodynamic forces (lift L and drag D) are functions of airspeed V, altitude h, and angle of attack α:

$$L = C_L(\alpha)\tfrac{1}{2}\rho V^2 S, \qquad D = C_D(\alpha)\tfrac{1}{2}\rho V^2 S \tag{12}$$

Since the trajectories under investigation involve relatively modest variations in altitude, the maximum thrust is assumed to be a function of airspeed only, i.e.,

$$T = \beta T_{\max}(V) \tag{13}$$

Although the aim of the present work is to extend the work of Miele et al. to flight in three dimensions, there are some slight modifications incorporated in the current model, of which the most significant one is related to modeling the angle-of-attack response. In the work of Miele et al.,[3] not only a bound is imposed on the maximum value the angle of attack α can attain, but also the rate of change of this variable is limited. In this work instantaneous angle-of-attack and roll-angle response is assumed. Although neglecting the $\dot{\alpha}$ constraint seems to be justified due to the fairly large time scale of flight, a validation effort that involves including the aircraft rotational inertia in roll and pitch in the system model is currently being undertaken.

Aerodynamic and Thrust Characteristics

In this study a Boeing 727 point-mass model has been used that has been adapted from a model originally developed by Miele et al. The main characteristics of this aircraft model are

$$T_{\max} = T_0 + T_1 V + T_2 V^2 \tag{14}$$

$$C_D = D_0 + D_1\alpha + D_2\alpha^2 \tag{15}$$

$$C_L = L_0 + L_1\alpha + L_2(\alpha - \alpha_{\text{ref}})^2 \tag{16}$$

Details of the aerodynamic and thrust data (for the aircraft in landing configuration) can be found in Refs. 10 and 11.

Microburst Wind Model

The microburst model used herein is an axisymmetric three-dimensional extension of the two-dimensional model presented in Ref. 10. Because of the axisymmetric character of the microburst model, it is convenient to use polar coordinates to describe the flow field in a horizontal plane (see Fig. 2). The induced radial and vertical wind velocities at any point in the three-dimensional space can be computed through the following relations:

$$W_r = f_r\left(\frac{100}{[(r - D/2)/200]^2 + 10} - \frac{100}{[(r + D/2)/200]^2 + 10}\right) \tag{17}$$

$$W_h = -f_h\left(\frac{0.4h}{(r/400)^4 + 10}\right) \tag{18}$$

where r is the radial distance from the microburst center (axis of symmetry) located at the point (x_c, y_c), i.e.,

$$r = \sqrt{(x - x_c)^2 + (y - y_c)^2} \tag{19}$$

Using polar coordinates, the horizontal wind components W_x and W_y can be readily related to the radial wind velocity W_r:

$$W_x = \cos\psi_w W_r(r), \qquad W_y = \sin\psi_w W_r(r) \tag{20}$$

where ψ_w is the direction of the radial wind velocity vector.

Note that in the present study the origin of the coordinate frame is located at the runway threshold. The parameter D in Eq. (17) specifies the diameter of the peak radial outflow-velocity contour (in this study D is always taken as 2000 m). The parameters f_r and f_h characterize the intensity of the horizontal shear and downdraft, respectively. In all examples presented here the parameters f_r and f_h have been set at the value 2. The wind profiles corresponding to the model given in Eqs. (17) and (18) are shown in Fig. 3 for the above-indicated values of the parameters. Note that the horizontal wind component W_r is only a function of the radial distance to the microburst center, whereas the vertical wind component W_h also depends on altitude to ensure that W_h decreases with decreasing altitude and satisfies the continuity condition, i.e., zero vertical windspeed at ground level. Clearly, the vertical windspeed model is valid at low altitudes only. Note that the wind model given by Eqs. (17) and (18) differs from the model used by Miele et al.[3] The present model has the (numerical-mathematical) advantage that it is very smooth.

An important characteristic parameter used in the evaluation of windshear performance is the so-called F factor.[1,7] Here we define this windshear hazard factor as

$$F \triangleq \frac{T - D}{W} - \frac{\dot{E}}{V} \tag{21}$$

Defining the F factor in this particular fashion permits its use in the analysis of both two- and three-dimensional windshear encounters. A comparison of Eqs. (4) and (21) reveals that the F factor can be readily interpreted as the loss or gain in available excess thrust-to-weight ratio due to the combined effect of downdraft and horizontal windshear. The F factor therefore represents a direct measure of the degradation of an aircraft's climb gradient capability at constant speed caused by the presence of windshear/downdraft. Note that positive values of the F factor indicate a performance-decreasing situation. Substitution of Eq. (4), combined with the use of polar horizontal position coordinates, allows the F factor in Eq. (21) to be conveniently expressed as

$$F = \frac{\cos\gamma}{g}\left\{V\cos\gamma\left[\frac{\partial W_r}{\partial r}\cos^2(\psi - \psi_w) + \frac{W_r}{r}\sin^2(\psi - \psi_w)\right] + W_r\frac{\partial W_r}{\partial r}\cos(\psi - \psi_w)\right\} + \frac{\sin\gamma}{g}\left\{\frac{\partial W_h}{\partial r}[W_r + V\cos\gamma \times \cos(\psi - \psi_w)] + \frac{\partial W_h}{\partial h}[W_h + V\sin\gamma]\right\} - \frac{W_h}{V} \tag{22}$$

It is noted that the F factor does not merely depend on the spatial location within the flow field, but rather on all state variables. In Fig. 4 the F factor is plotted as a function of the radial distance r and the relative wind direction $(\psi_w - \psi)$, using values for altitude, speed, and flight path angle representative of a final approach. It is observed that for the present wind model the peak value of the F factor is not generally reached at the center of the microburst but rather at some distance away from the center. It can be seen that outside the peak velocity contour an energy gain due to windshear can be achieved. When an aircraft is flying outside the peak radial outflow-velocity contour, the best performance is achieved by flying along a "wind radial."

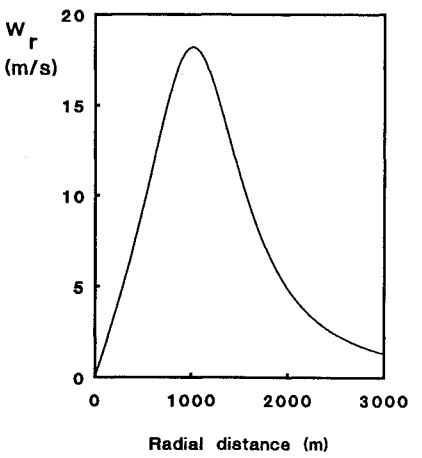

a)

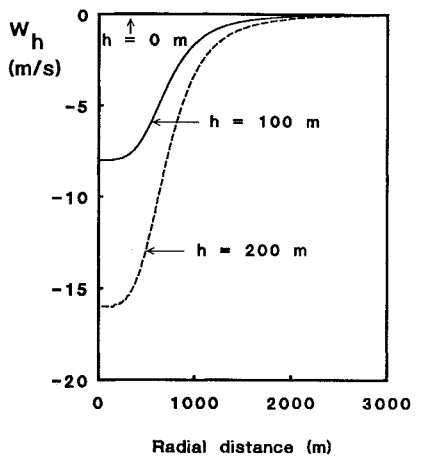

b)

Fig. 3 Horizontal and vertical wind velocity profiles.

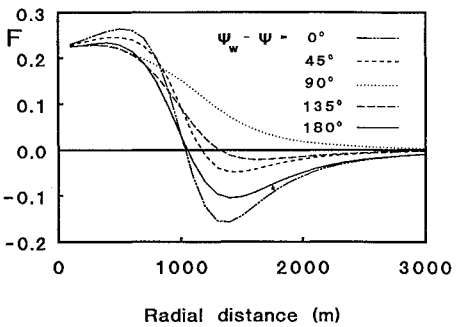

Fig. 4 F factor as function of radial distance r for several values of relative wind direction $(\psi_w - \psi)$, where it is assumed that altitude $h = 100$ m, airspeed $V = 70$ m/s, and flight path angle $\gamma = -3$ deg.

III. Optimal Control Formulation

Optimization Criterion

Similar to Ref. 3, the objective in this study is to maximize the minimum altitude reached by an aircraft at any point along the trajectory, or, in other words, to minimize the peak value of the altitude drop:

$$I^* = \min I = \min\left[\max_t(h_{\text{ref}} - h(t))\right] \tag{23}$$

Following the approach of Ref. 3, the minimax criterion in Eq. (23) (Chebyshev performance index) is approximated by a Bolza performance index:

$$J^* = \min J = \min\int_0^{t_f}(h_{\text{ref}} - h)^n\,dt \tag{24}$$

where n is a large, positive, even exponent. Note that for the best possible computational results, the reference altitude h_{ref} should be chosen as small as possible but such that the right-hand side of Eq. (23) remains positive at all times. The numerical values of the constants in Eq. (24) that have been used here are $n = 6$ and $h_{ref} = 400$ m.

It is noted that, in addition to the above approximation, it is also possible to apply another transformation technique that can solve the original minimax problem (23). More specifically, the minimax problem can be converted into an equivalent optimal control problem with state-variable inequality constraints.[12,13] In conjunction with the presently used multiple-shooting algorithm,[11] this technique appears to be well suited for numerical treatment of the multipoint boundary-value problem that arises from the optimal control analysis. Although this approach is mathematically rather complicated, it certainly merits further consideration in future research.

Boundary Conditions

The following initial conditions (at which the escape procedure is commenced) have been assumed in this study:

$$x(0) = x_0 = -2500 \text{ m}, \qquad y(0) = y_0 = 0 \text{ m},$$

$$h(0) = h_0 = 131 \text{ m}$$

$$E(0) = E_0 = 384.326 \text{ m}, \qquad \gamma(0) = \gamma_0 = -3 \text{ deg},$$

$$\psi(0) = \psi_0 = 0 \text{ deg}$$

$$\beta(0) = \beta_0 = 0.333$$

These values correspond to a situation in which an aircraft would fly during a stabilized approach ($V = 70.5$ m/s) without winds. It needs to be realized that, in the presence of winds, the required values for γ_0 and β_0 will be somewhat different. However, since different locations of the microburst will be considered in the numerical examples, the above-stated values will be assumed to apply in all situations, merely to achieve some degree of consistency.

No terminal boundary conditions on the state variables have been formally imposed, implying that the terminal value of each adjoint variable is zero. Specifying a terminal state would mainly affect the extremal solution in the aftershear region.[13] Our primary interest is in the control behavior during the passage of the shear region.

In the present work, for a given encounter, the final time t_f is selected such that a terminal value of 300 m is achieved for altitude. This warrants that at all times altitude remains well below the specified value of h_{ref} in the performance index of Eq. (24) while ensuring that in all cases the high-shear region can be completely traversed.

Necessary Conditions for Optimality

To summarize, the optimal control problem to be solved is to determine the optimal controls β^*, μ^*, and α^* such that starting from the initial conditions, the performance index of Eq. (24) is minimized.

Application of the first-order necessary conditions of optimal control theory to the above-stated problem results in a two-point boundary-value problem (TPBVP), which is highly unstable and therefore rather difficult to solve. In the present study the extremals (solutions to the TPBVP) have been obtained iteratively using a very accurate multiple-shooting algorithm.[11] At this point it is important to note, however, that such extremal solutions are merely candidates for local optimality. As a matter of fact, we have been able to find up to three extremals for a given set of boundary conditions in most cases. It is imperative to verify local optimality of these candidate extremals by checking for the second-order necessary conditions (Jacobi test). Such a test, together with the Legendre-Clebsch condition (which is easily verified), can provide assurance concerning the local optimality of candidate extremals. We emphasize, however, that, as yet, we have only concerned ourselves with computing candidate extremals.

IV. Extremal Solutions

Baseline Scenario

In order to investigate the characteristic features of the optimal escape trajectories, the principal parameters that have been varied in this study are the position coordinates (x_c, y_c) of the microburst center. The reference situation that has been selected to serve as a baseline scenario concerns a microburst of which the center is located at (−1500 m, 0 m). This implies that for the given initial conditions an aircraft in straight flight will fly exactly along the x axis of the reference frame (see Fig. 3), passing right through the microburst center. Relative to this "symmetric" reference situation both the distance of the microburst center to the runway threshold (x_c coordinate position) and the lateral offset distance y_c have been varied.

In Fig. 5 the results pertaining to the baseline scenario have been summarized. For any given (nonzero) value of the aerodynamic roll-angle limit, it has been possible to compute three different extremals. Due to the symmetry in the geometry of this microburst encounter, it is not really surprising that the first converged extremal that was obtained simply was the optimal trajectory established earlier in a two-dimensional analysis,[10] i.e., a straight flight along the x axis, during which an aircraft does not experience any cross-wind. Subsequent efforts focused on the computation of lateral-escape trajectories. To demonstrate the impact of the aerodynamic roll-angle limit on the solution behavior, three different values for the roll-angle limit have been considered in Fig. 5, namely 15, 20, and 25 deg. Due to symmetry considerations it is clear that lateral-escape maneuvers can be performed by making either a left or a right turn.

Figure 5a shows the ground tracks for the escape maneuvers. It is noted that for the considered reference situation the location of the microburst center is such that the initial conditions for the trajectories are on the maximum radial outflow velocity contour.

Figures 5b and 5c show the time histories for the two control variables, angle of attack and aerodynamic roll angle. It is evident that all escape maneuvers are performed at full throttle. The behavior demonstrated by the turning extremals is fairly transparent. The relatively high initial angle of attack for a lateral maneuver results in a relatively high lift and drag. The increase in lift not only leads to a high turn rate but also results in an initial "zoom climb," as can be observed in Fig. 5d. Obviously, airspeed is reduced in the initial phase (see Fig. 5e). Clearly, an initial high turn rate is desired to direct the aircraft away from the microburst center, such as to obtain a positional advantage within the wind flow field. On the other hand, it is also desirable to keep the energy bleed-off rate (and thus drag) as modest as possible. The optimization process attempts to establish the overall best compromise between those two conflicting requirements.

It is noted that there is a close correspondence between the angle-of-attack behavior and the F-factor behavior (Fig. 5f). For example, maximum angle of attack is generally reached at the end of high-shear region (region with high F values). In Ref. 7 a microburst is classified as hazardous if the average F factor exceeds 0.1 over any 1-km segment. Using this as a yardstick, it is readily clear that the microburst encounter considered here easily qualifies as hazardous. Figure 5f also makes clear that turning the aircraft away from the microburst center does not necessarily lead to a reduction in the peak value of the F factor, but rather the high-shear region is passed much quicker.

Figure 5g shows the typical behavior of the corresponding heading angle time history for one extremal. Generally speaking it can be observed that, in the final stage of a lateral-escape maneuver (i.e., in the aftershear region), an aircraft ends up flying along a "horizontal wind radial." This particular behavior has already been explained in the analysis of the F-factor plot (Fig. 4) in the previous section. Based on this behavior, closed-loop lateral-escape strategies are currently being developed.[11,14] In particular, a constant-pitch technique is examined in combination with a simple guidance law for the aerodynamic roll angle, which involves the feedback of the heading error (i.e., the difference between the radial wind direction and the actual heading).

The improvements in performance that can be obtained by executing a lateral-escape maneuver are significant, as can be observed

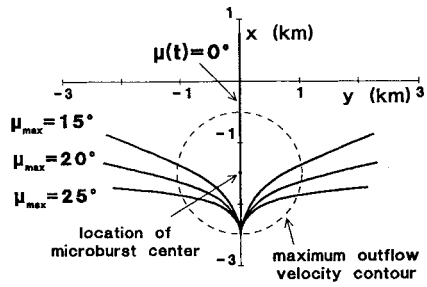

a)

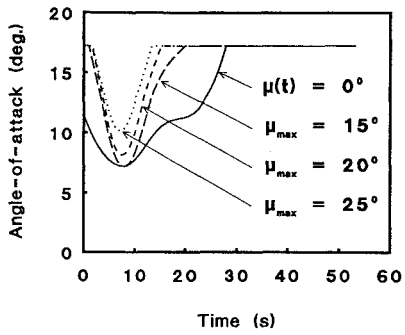

b)

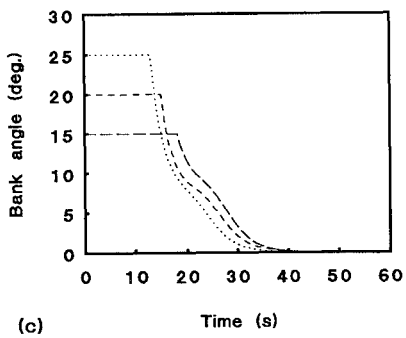

(c)

c)

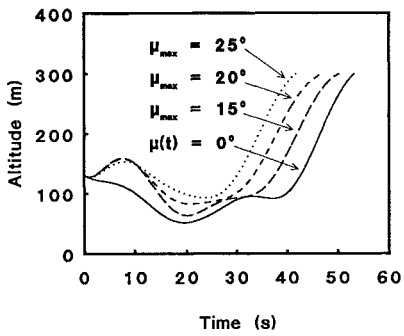

d)

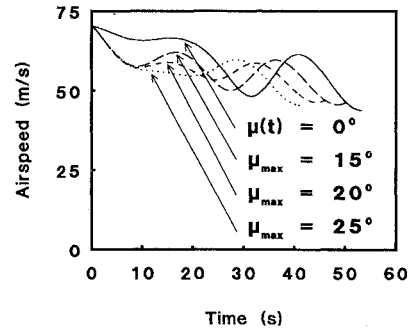

e)

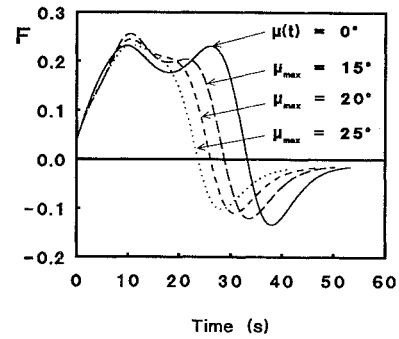

f)

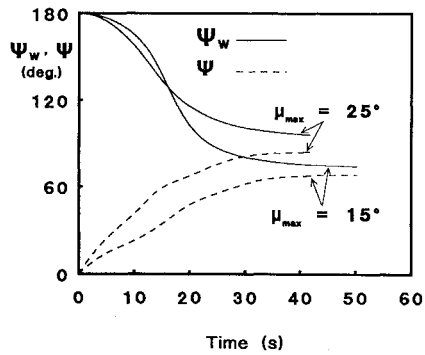

g)

Fig. 5 Comparison of extremal solutions for various values of roll-angle limit. Distance of microburst center to runway threshold is 1500 m. No lateral displacement.

from Fig. 5d. The results for the baseline scenario clearly indicate that a large value of the aerodynamic roll-angle limit is desirable. This result seems to contradict the findings of Ávilo de Melo and Hansman,[8] who claim that large roll angles tend to deteriorate the performance when an aircraft is deep in the shear region. However, at this point it is recalled that, unlike the optimal maneuvers established herein, the lateral-escape maneuvers proposed in Ref. 8 are performed using a constant roll angle until a heading change of 90 deg has been achieved.

In addition to comparing the minimum altitudes achieved in turning and nonturning escape trajectories, also some alternative ways to express the performance improvements have been examined. For example, the minimum altitude achieved in a lateral-escape maneuver with an aerodynamic roll-angle limit of 15 deg is about 12 m higher than the minimum altitude achieved in an escape maneuver with roll angle fixed at zero. This corresponds to a reduction in the required advance warning time of about 2.1 s. This result has been obtained by delaying the initiation of the lateral-escape maneuver while proceeding along the glideslope, such that the resulting minimum altitude is equal to the minimum altitude obtained for the nonturning trajectory. Alternatively, the lateral-escape maneuver can be flown with a 7.5% increase in the windshear intensity and still achieve the same performance as the nonturning trajectory.

Effect of a Lateral Microburst Displacement

A second numerical example of extremal behavior concerns a situation in which the center of the microburst is offset from the x axis of the reference frame. More specifically, the lateral microburst displacement y_c is set to 100 m in this example. The results are illustrated in Fig. 6. The ground tracks shown in Fig. 6a no longer exhibit a symmetry relative to the x axis. In other words, there is now a need to distinguish between left and right turns. However, we still have the situation that there are generally three different extremals for a given value of the roll-angle limit (provided this value is sufficiently large, as will be shown).

First of all, there is an extremal that, as in the baseline scenario, passes right through the microburst center. This extremal has been labeled unconstrained, to indicate that only some modest initial rolling

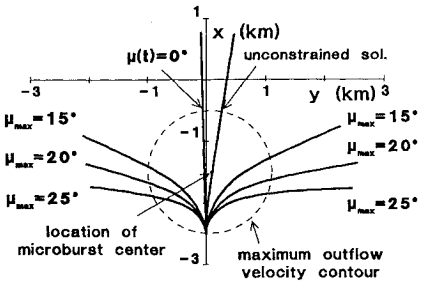

a)

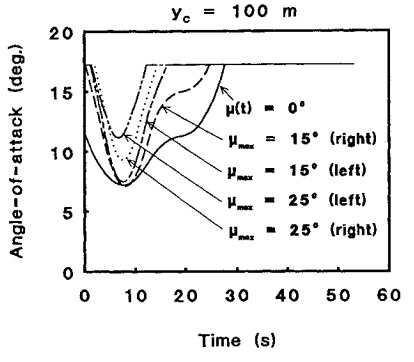

b)

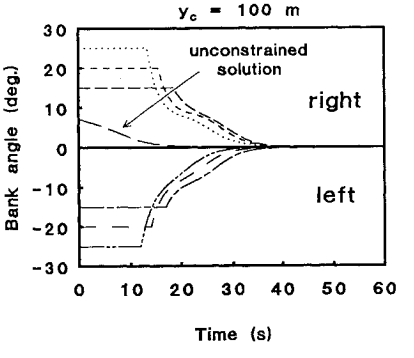

c)

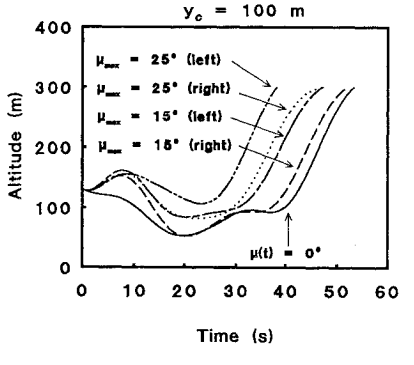

d)

is required (see Fig. 6c). A second type of extremal concerns escape trajectories involving a turn to the right, or, in other words, a turn toward the microburst center. Finally, a third type of extremal that can be found concerns trajectories featuring a turn to the left, or, in other words, a turn away from the microburst center. For a given value of the roll-angle limit, the optimal angle-of-attack behavior is quite different for a left and a right turn, as can be observed from Fig. 6b, where results are shown for a roll-angle limit of 15 deg and 25 deg. For reference also a trajectory with aerodynamic roll-angle fixed at 0 deg has been included in Fig. 6.

Not surprisingly, escape maneuvers to the left, in which aircraft are turned away from the microburst center, lead to a much better

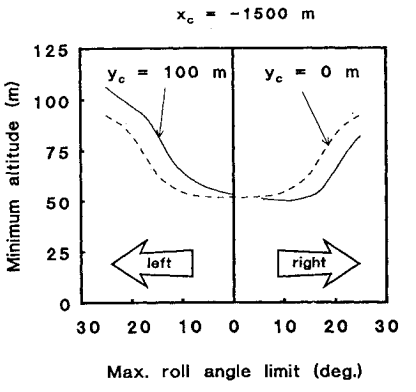

e)

Fig. 6 Comparison of extremal solutions for various values of roll-angle limit. Distance of microburst center to runway threshold is 1500 m. Lateral displacement $y_c = 100$ m.

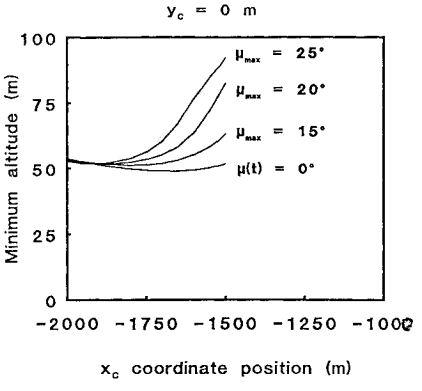

Fig. 7 Minimum altitude as function of distance of microburst center to runway threshold. No lateral displacement.

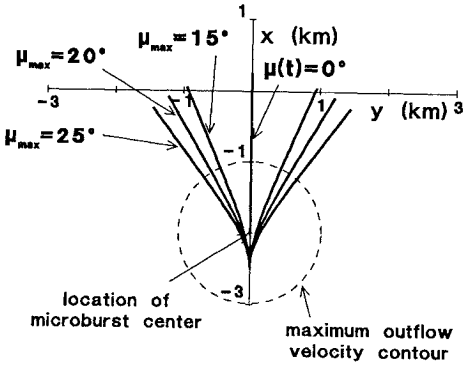

Fig. 8 Ground tracks of extremal solutions for various values of roll-angle limit. Distance of microburst center to runway threshold is 2000 m. No lateral displacement.

performance. In fact, Fig. 6d makes clear that, for an aerodynamic roll-angle limit of 15 deg, turning to the right may even lead to a lower minimum altitude than not turning at all. Figure 6e shows the minimum altitude reached at any point along the trajectory as a function of the specified roll-angle limit.

Note that the curve in this figure pertaining to the present example is interrupted. The reason for this is that it proved to be impossible to compute escape trajectories that involve a turn to the right, but pass left of the microburst center. For the purpose of comparison, the results for the baseline scenario have been included in Fig. 6e as well.

Effect of Longitudinal Microburst Displacement

This particular example serves to demonstrate the effect of displacing the center of the microburst in longitudinal direction. As in the baseline scenario, a symmetric encounter is considered, i.e., the

microburst center is located on the x axis of the reference frame. Figure 7 presents the minimum altitude reached at any point along the trajectory as a function of the longitudinal position of the microburst center for several values of the aerodynamic roll-angle limit. The results shown in Fig. 7 confirm the findings of Ávilo de Melo and Hansman,[8] that lateral maneuvering is less effective if the maneuver is initiated deep in the microburst core.

Figure 8 shows the ground tracks of example trajectories start well within the peak radial outflow velocity contour, i.e., $x_c = -2000$ m. Since the aerodynamic roll angle leaves its limit after only just a few seconds, the total heading change for the lateral-escape maneuvers is actually rather modest. As a result, the differences in performance between lateral- and non-lateral-escape maneuvers are not very large either.

V. Conclusions

Optimal lateral-escape trajectories in a microburst wind field were studied for an aircraft on final approach. Provided that the center of the microburst is not too far offset from the centerline extension of the approach runway, typically three extremal solutions can be found, namely one trajectory passing the microburst center to the left, one trajectory passing the center to the right, and one passing right through the center.

If the aircraft turns away from the microburst center and the maneuver is initiated not too close to the microburst center, lateral maneuvering may lead to a significant improvement in the aircraft's escape capability. On the other hand, lateral maneuvering was shown to be less beneficial if the escape maneuver is commenced deep inside the high-shear region. In case of a nonsymmetric microburst encounter, incorrect lateral maneuvering (toward the microburst center) may result in a performance loss.

One of the most striking results established in this study relates to the energy management features of lateral maneuvering. In an optimal lateral-escape maneuver the best overall compromise between the conflicting requirements of a high initial turn rate (to take the aircraft away from the microburst center) and a low-energy bleed-off rate (to maintain climb-gradient capability) is established. The relatively high lift needed to produce a high turn rate also leads to an initial climb, rather than a descent, in a lateral-escape maneuver.

Currently, research efforts are underway that exploit the insight obtained from the present analysis to develop feedback guidance laws that approximate the open-loop optimal lateral-escape trajectories. Preliminary results are quite encouraging.[11,14]

An important issue that needs to be addressed relates to the response characteristics of the current control variables angle of attack and roll angle. In particular, it will be of considerable interest to find out to what extent the advantages of the lateral escape vis-à-vis the longitudinal escape can be preserved if the aircraft rotational inertia in roll and pitch are included in the system model.

It is clear that a substantial research effort is still required before it is meaningful to address operational issues, such as potential conflicts with the requirements of air traffic control.

References

[1]Miele, A., Wang, T., and Melvin, W. W., "Optimization and Acceleration Guidance of Flight Trajectories in a Windshear," *Journal of Guidance, Control, and Dynamics*, Vol. 10, 1987, pp. 368–377.

[2]Miele, A., Wang, T., and Melvin, W. W., "Penetration Landing Guidance Trajectories in the Presence of Windshear," *Journal of Guidance, Control, and Dynamics*, Vol. 12, 1989, pp. 806–814.

[3]Miele, A., Wang, T., Melvin, W. W., and Bowles, R. L., "Acceleration, Gamma and Theta Guidance for Abort Landing in a Windshear," *Journal of Guidance, Control, and Dynamics*, Vol. 12, 1989, pp. 815–821.

[4]Zhao, Y., and Bryson, A. E., "Optimal Paths Through Downbursts," *Journal of Guidance, Control, and Dynamics*, Vol. 13, 1990, pp. 813–818.

[5]Zhao, Y., and Bryson, A. E., "Control of an Aircraft in Downbursts," *Journal of Guidance, Control, and Dynamics*, Vol. 13, 1990, pp. 819–823.

[6]Hinton, D. A., "Forward-Look Wind-Shear Detection for Microburst Recovery," *Journal of Aircraft*, Vol. 29, 1992, pp. 63–66.

[7]Bowles, R. L., "Reducing Windshear Risk Through Airborne Systems Technology," *Proceedings of the 17th Congress of the International Council of the Aeronautical Sciences*, Vol. 2, Stockholm, Sept. 1990, pp. 1603–1630.

[8]Ávila de Melo, D., and Hansman, R. J., "Analysis of Aircraft Performance During Lateral Maneuvering for Microburst Avoidance," *Journal of Aircraft*, Vol. 28, 1991, pp. 837–842.

[9]Federal Aviation Administration Windshear Training Aid, U.S. Dept. of Transportation, Associate Administration for Development and Logistics, Washington DC, 1987.

[10]Soesman, J. L., "Control of Aircraft Through Windshear During Final Approach," National Aerospace Laboratory TR 90117 L, The Netherlands, 1990.

[11]Visser, H. G., "Optimal Lateral Escape Maneuvers for Microburst Encounters During Final Approach," Delft University, Rept. LR-691, July 1992.

[12]Bulirsch, R., Montrone, F., and Pesch, H. J., "Abort Landing in the Presence of Windshear as a Minimax Optimal Control Problem, Part 1: Necessary Conditions," *Journal of Optimization Theory and Applications*, Vol. 70, 1991, pp. 1–23.

[13]Bulirsch, R., Montrone, F., and Pesch, H. J., "Abort Landing in the Presence of Windshear as a Minimax Optimal Control Problem, Part 2: Multiple Shooting and Homotopy," *Journal of Optimization Theory and Applications*, Vol. 70, 1991, pp. 223–254.

[14]Visser, H. G., "Optimal Lateral Maneuvering for Microburst Encounters During Final Approach," *Proceedings of the 18th Congress of the International Council of the Aeronautical Sciences*, Vol. 2, Beijing, Sept. 1992, pp. 1587–1597.